Phase diagram of amorphous solid water: Low-density, high-density, and very-high-density amorphous ices

Nicolas Giovambattista,[1,2] H. Eugene Stanley,[2] and Francesco Sciortino[3]
[1]*Department of Chemical Engineering, Princeton University, Princeton, New Jersey 08544-5263 USA*
[2]*Center for Polymer Studies and Department of Physics, Boston University, Boston, Massachusetts 02215 USA*
[3]*Dipartimento di Fisica and INFM Udr and SOFT: Complex Dynamics in Structured Systems, Universita' di Roma "La Sapienza" – Piazzale Aldo Moro 2, I-00185, Roma, Italy*
(Received 21 February 2005; published 30 September 2005)

We calculate the phase diagram of amorphous solid water by performing molecular dynamics simulations using the extended simple point charge (SPC/E) model. Our simulations follow different paths in the phase diagram: isothermal compression/decompression, isochoric cooling/heating, and isobaric cooling/heating. We are able to identify low-density amorphous (LDA), high-density amorphous (HDA), and very-high density amorphous (VHDA) ices. The density ρ of these glasses at different pressure P and temperature T agree well with experimental values. We also study the radial distribution functions of glassy water. In agreement with experiments, we find that LDA, HDA, and VHDA are characterized by a tetrahedral hydrogen-bonded network and that, as compared to LDA, HDA has an extra interstitial molecule between the first and second shell. VHDA appears to have two such extra molecules. We obtain VHDA, as in experiment, by isobaric heating of HDA. We also find that "other forms" of glassy water can be obtained upon isobaric heating of LDA, as well as amorphous ices formed during the transformation of LDA to HDA. We argue that these other forms of amorphous ices, as well as VHDA, are not altogether new glasses but rather are the result of aging induced by heating. Samples of HDA and VHDA with different densities are recovered at normal P, showing that there is a continuum of glasses. Furthermore, the two ranges of densities of recovered HDA and recovered VHDA overlap at ambient P. Our simulations reproduce the experimental findings of HDA→LDA and VHDA→LDA transformations. We do not observe a VHDA→HDA transformation, and our final phase diagram of glassy water together with equilibrium liquid data suggests that for the SPC/E model the VHDA→HDA transformation cannot be observed with the present heating rates accessible in simulations. Finally, we discuss the consequences of our findings for the understanding of the transformation between the different amorphous ices and the two hypothesized phases of liquid water.

DOI: 10.1103/PhysRevE.72.031510 PACS number(s): 61.43.Fs, 61.43.Bn, 61.20.Ja

I. INTRODUCTION

Liquids can transform into glass if they are cooled fast enough to avoid crystallization. Water is not an exception, although vitrifying liquid water requires very high quenching rates ($\approx 10^6$ K/s) [1] — the resulting glass is called hyperquenched glassy water (HGW). Actually, water can exist in more than one amorphous form, a property called "polyamorphism" [2–4]. Uniaxial compression of ice-I_h [5] or ice-I_c [6,7] at temperature $T=77$ K to pressures $P \gtrsim 1$ GPa produces a disordered high-density material named high-density amorphous ice (HDA). If HDA is recovered at $T=77$ K and $P=1$ bar and then heated isobarically, it transforms irreversibly at $T \approx 125$ K to a disordered low-density material named low-density amorphous ice (LDA) [5,8]. Both HGW and LDA transform to HDA when compressed at $T=77$ K at $P=0.6$ GPa [8–10]. X-ray and neutron diffraction measurements suggest that LDA is structurally identical to HGW [11] and, although small differences have been found [12–14], the common view is that HGW and LDA are the same material [2,4,15].

The LDA-HDA transformation is reversible if it is performed above $T \approx 130$ K [16]. Furthermore, because the LDA-HDA transformation is very sharp and shows hysteresis, it has been suggested that it is a first-order transition [16,17]. It has also been proposed [18] to interpret the LDA-HDA transition as the glass counterpart of the first-order transition between two liquids of different structure, the liquid-liquid phase transition scenario [19]. In this view, LDA is the glass associated with a low-density liquid (LDL) while HDA is the glass associated with a high-density liquid (HDL) [17–22].

Computer simulations have been able to reproduce many of the experimental results. More than 15 years ago, simulations using the TIP4P model found a transformation of ice-I_h into HDA when compressed at $T=80$ K and a transformation of HDA to LDA upon isobaric heating at zero P [23]. The LDA-HDA reversible transformation is also found in simulations using the ST2 [19] and TIP4P [18] models. Computer simulations in the liquid phase also show a LDL-HDL first-order transition [19,24–26].

Very recently, a glass denser than HDA was identified in experiments, and named very-high-density amorphous (VHDA) ice [27,28]. VHDA is obtained by isobaric heating at high P of HDA from $T=77$ K to $T \approx 165$ K. Two samples of HDA, one heated isobarically at $P=1.1$ GPa and the other at $P=1.9$ GPa, both relax at $T=77$ K and $P=1$ bar to the same structure with a density of $\rho=1.25\pm0.01$ g/cm^3, i.e., $\approx 9\%$ denser than HDA ($\rho=1.15$ g/cm^3) and $\approx 40\%$ denser than LDA ($\rho=0.94$ g/cm^3). It appears that the properties of

HDL are closer to VHDA than to HDA [29,30]. In recent reports [31,32], it has been shown that VHDA can be obtained in computer simulations by following the same procedure as in experiments. Further, we argued [32] that VHDA may not be a new glass different than HDA, but rather VHDA results from partial annealing of the "more stable" HDA structure. Further, our simulations also show that VHDA (and not HDA) is the glass obtained by isobaric quenching of the equilibrium liquid at high P.

It is an open question whether all forms of glassy water can be classified into two amorphous forms, which we call LDA and VHDA. While this might be the case for glasses obtained by cooling liquid water or compressing ice, there are many different experimental techniques to obtain glassy water. For instance, amorphous ice can be also obtained by exposing crystalline ice to radiations such as electrons [33], ultraviolet photons [34], and ion bombardment [35]. The situation is more complicated when considering the effect of aging in the glassy state. Recent works [36–38] suggest that aging takes place on the experimental time scale when HDA is kept at ambient P and T is below the HDA-LDA transformation T. The ρ and structure of the sample changes with the annealing T and annealing time.

In this work we rebuild the phase diagram of amorphous water on the basis of simulations using the extended simple point charge (SPC/E) model. Our simulations consist mainly of isobaric cooling/heating and isothermal compression/decompression cycles. In Sec. II, we describe briefly the simulation details. In Sec. III, we show that compression of LDA leads to HDA. Isobaric heating at different P's is reported in Sec. IV, where the HDA$\rightarrow$VHDA transformation is also described. In Sec. V, we describe the results of recovering HDA and VHDA at normal P. The structures of all glasses are studied in Sec. VI. The HDA$\rightarrow$LDA, VHDA$\rightarrow$LDA, and VHDA$\rightarrow$HDA transitions are investigated in Sec. VII. Finally, in Sec. VIII we discuss our results and recent experiments in the context of a possible first-order transition line separating two amorphous ices at low T, and two liquid phases at high T.

II. SIMULATIONS

We perform molecular dynamics (MD) simulations using the extended simple point charge (SPC/E) model of water [39]. This model has been extensively used to study the thermodynamics [40,41] and dynamics [42,43] of liquid water. Thermodynamic and dynamical properties of SPC/E water are well known, and are consistent with experimental facts. The SPC/E model reproduces the thermodynamic anomalies characterizing water (e.g., it shows a maximum in ρ [44]). This model has also been used to study glassy water, and is able to produce glassy states corresponding to LDA, HDA, and VHDA [32,45]. Here, we simulate a system of $N=216$ molecules [46], and average the results over 16 independent trajectories. We use periodic boundary conditions. Long range forces are treated using the reaction field method with a cutoff of 0.79 nm. No long range corrections for the Lennard-Jones interactions are added to both the energy and pressure.

To study the phase diagram of glassy water we perform three different kinds of simulations: (i) isobaric cooling/heating, (ii) isochoric cooling/heating, and (iii) isothermal compression/decompression.

During cooling/heating at both constant ρ or P, we change T by rescaling the velocities of the molecules. At every time step $\delta t=1$ fs, we increase the T by $\delta T=q\delta t$, where q is the cooling/heating rate and $q=\pm 3\times 10^{10}$ K/s. These values for q have been used in previous simulations to study the effect of cooling and heating rates on the glass transition temperature $T_g=T_g(P)$ [47,48]. The glass obtained with a cooling rate $q=-3\times 10^{10}$ K/s behaves, upon heating at $q=+3\times 10^{10}$ K/s, as a slow-cooled glass as found in experiments showing no signs of hyperquenching effects. On the other hand, the lowest cooling/heating rates accessible nowadays in computer simulations are $|q|\approx 10^{10}$ K/s [30].

For the compression/decompression simulations at $T>0$ K we perform MD simulations at constant ρ for intervals of 1 ps. At the end of each interval of 1 ps, we increase ρ by $\delta\rho=\pm 5\times 10^{-5}$ g/cm^3, so our compression/decompression rate is $\delta\rho/\delta t=\pm 5\times 10^{-5}$ g/cm^3/ps. This value was already used to study the potential energy landscape for the LDA-HDA transformation [45]. These ρ changes are performed by rescaling isotropically the coordinates of the molecular center of mass. For the compression simulations at $T=0$ K, at each simulation step we change ρ by $\delta\rho=\pm 5\times 10^{-5}$ g/cm^3 and then minimize the energy. At each step ρ is modified by rescaling isotropically the center of mass of each molecule.

III. LDA-HDA TRANSFORMATION

We prepare LDA by hyperquenching at constant $\rho=0.9$ g/cm^3 liquid configurations obtained at $T=220$ K. We have chosen a glass obtained quenching a low T liquid configuration—i.e., properly speaking a HGW—at $\rho=0.9$ g/cm^3 as starting LDA structure to guarantee that the chosen configuration is a low ρ glass with an optimized tetrahedral network of hydrogen bonds. To obtain HDA, we compress LDA at constant T [45] from $\rho=0.9$ g/cm^3 to $\rho>1.5$ g/cm^3. The T is fixed at $T=0$, 77, 100, 120, 140, 160, and 170 K. These T are below the melting temperature $T_m\approx 220$ K (as estimated in Ref. [49]) and below $T_g(P)$. Evaluation of the specific heat upon heating the glass with a heating rate of $q=+3\times 10^{10}$ K/s to the liquid phase indicates that $T_g(P)>170$ K for all P's studied.

In Fig. 1 we show $P(\rho)$ during isothermal compression at four of the simulated T. We also show equilibrium data taken from the liquid phase simulations reported in Ref. [18]. From Fig. 1 we note:

(1) For all $T\leqslant 170$ K isotherms show a transformation from LDA to HDA. The linear increase of $P(\rho)$ crosses to a transition region around $\rho'\approx 1.03$ g/cm^3 and $P'\approx 0.7$ GPa for $T=0$ K and $\rho'\approx 0.97$ g/cm^3 and $P'\approx 0.13$ GPa for $T=170$ K. The LDA-HDA transition starts at higher ρ and P on decreasing T. This feature has been observed in computer simulations of different models of water, including ST2 [19,18] and TIP4P [18], and agrees with experiments [16,50].

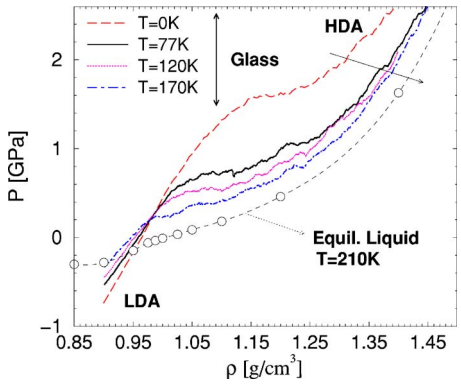

FIG. 1. (Color online) Transformation of LDA to HDA obtained by isothermal compression at $T=0$, 77, 120, and 170 K. LDA was obtained by hyperquenching at constant ρ equilibrium liquid configurations at $T=220$ K and $\rho=0.9$ g/cm^3. The transformation starts approximately at $\rho'=1.03$ g/cm^3, $P'=0.7$ GPa at $T=0$ K and shift with T to $\rho'=0.97$ g/cm^3, $P'=0.13$ GPa at $T=170$ K. We also show data for equilibrium liquid at $T=210$ K (from Ref. [18]), one of the lower T accessible for equilibrium liquid simulations. We note that glass isotherms cross at $\rho\approx0.98$ g/cm^3, $P\approx0.2$ GPa and that as T increases, the glass isotherms approach the liquid isotherm.

(2) All the compression curves at $T>0$ K collapse to a single curve at very high ρ, suggesting that there is a single HDA state at *very* high P. This is not the case for LDA because the P of LDA while compressing at $\rho=0.9$ g/cm^3 depends on T. Furthermore, a study of the potential energy landscape during the LDA-HDA transformation shows clear differences between two LDA samples at low P and T [45].

(3) The isotherms in the glassy states cross each other at approximately $\rho=0.98$ g/cm^3 and $P=0.2$ GPa (see also Fig. 5). This could suggest (if these out of equilibrium isotherms could be interpreted as an effective equation of state of the glass) that ρ increases upon isobaric heating the glass at high P, while ρ decreases upon isobaric heating the glass at low P.

(4) We note that as the compression temperature increases from $T=0$ K to $T=170$ K the isotherms in the glassy state approach the liquid isotherm for $T=210$ K. Accordingly, we see that at low ρ (LDA, e.g., $\rho=0.9$ g/cm^3) increasing T increases P, while at high ρ (HDA, e.g., at $\rho=1.3$ g/cm^3) increasing T decreases P.

IV. ISOBARIC HEATING OF GLASSY WATER. VERY-HIGH-DENSITY AMORPHOUS ICE AND "OTHER" AMORPHOUS ICES

A. Heating at high P

Experimentally, VHDA is obtained by isobaric heating of HDA ($T=77$ K, $\rho=1.33$ g/cm^3) at $P=1.1$ GPa and HDA $T=77$ K, $\rho=1.45$ g/cm^3 at $P=1.9$ GPa [27]. The products are VHDA ($T\approx160$ K, $\rho\approx1.37$ g/cm^3) and VHDA ($T\approx177$ K, $\rho\approx1.51$ g/cm^3), respectively. Simulations with the SPC/E model also show a transformation between HDA to another glassy state identified with VHDA [32]. These

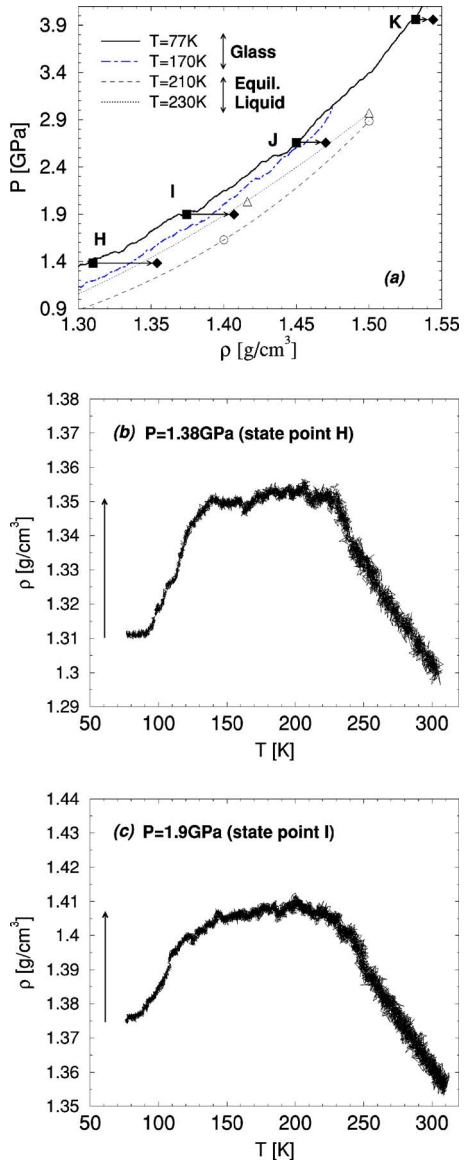

FIG. 2. (Color online) (a) Magnification of Fig. 1 corresponding to densities of HDA. To test the presence of VHDA we heat at constant P configurations corresponding to state points H, I, J, and K in the figure (see also Table I). Upon heating from $T=77$ K (squares) up to $T\approx170$ K (diamonds), the four state points move to higher densities crossing the glass isotherm for $T=170$ K and approaching the $T=210$ K liquid isotherm (see arrows). (b),(c) Examples of the evolution of ρ upon isobaric heating configurations of HDA indicated by the state points H, I, J, K in (a). In all cases, ρ increases with T before the liquid phase is reached. The denser glass to which HDA transforms is identified as the VHDA obtained in experiments. Arrows indicate the increase in ρ when heating the glass from $T=77$ K up to $T\approx170$ K. The increase in ρ is smaller as P increases.

simulations also suggest that HDA and VHDA are not different glasses, but rather that VHDA is the result of the relaxation of HDA upon heating. Furthermore, it is found that VHDA is the same glass obtained by cooling HDL [30,32].

TABLE I. Location in the P-ρ plane of the starting configurations used during the isobaric heatings. State points A–D correspond to LDA configurations while state points H–K represent HDA configurations. State points E–G correspond to configurations in the LDA-HDA transformation.

Label	ρ [g/cm^3]	P [GPa]
A	0.90	−0.55
B	0.94	−0.17
C	0.96	0.01
D	1.005	0.41
E	1.065	0.68
F	1.17	0.84
G	1.255	1.10
H	1.311	1.38
I	1.375	1.90
J	1.452	2.66
K	1.532	3.96

We obtain HDA by compressing LDA at $T=77$ K as explained in the last section. We confirm the transformation of HDA to a denser glass by isobaric heating of HDA at different P's. The HDA configurations correspond to four different states, indicated by state points H, I, J, and K in Fig. 2(a) (see Table I). For the four cases studied, ρ increases when heating the glass from $T=77$ K to $T\approx 170$ K, still below $T_g(P)$ [see, e.g., Figs. 2(b) and 2(c)]. On increasing T, the glass melts to the equilibrium liquid. The ρ increase is smaller the higher the P and it is indicated by arrows in Fig. 2(a). Note that the increase in ρ of ≈ 0.04 g/cm^3 that we find at $P=1.38$ GPa is very close to the estimated experimental values [27] of 0.04 and 0.06 g/cm^3 for isobaric heating at $P=1.1$ and $P=1.9$ GPa, respectively.

The $\rho(T)$ values shown in Figs. 2(b) and 2(c) at high T are the ones obtained in the equilibrium liquid. Indeed, at $P=1.38$ GPa and $T=230$ K the relaxation time is $\tau \approx 100$ ps [51]. Heating at a rate of $q_h=3\times 10^{10}$ K/s, the T change during 100 ps is about 3 K. Therefore, the system has time to relax before T changes considerably and the ρ measured is the same as in the equilibrium liquid. The decrease of ρ observed in Figs. 2(b) and 2(c) for $T\geqslant 230$ K (in the liquid phase) is in agreement with the location of the isotherms for $T=210$ K and $T=230$ K at high P shown in Fig. 2(a).

Computer simulations show that the final glass connected to the liquid phase by cooling at high P is VHDA [32]. We argue [32] that HDA is less stable than VHDA and it is a kinetically trapped glass that could not relax during the compression of LDA. The hypothesis that HDA is a kinetically trapped glass was already proposed based on recent computer simulations performed with the TIP4P model [31] and it was originally proposed by Mishima who observed that HDA samples (made by different P-T conditions) heated or annealed to 130–150 K at 1–1.5 GPa were characterized by identical x-ray patterns [52]. To provide further support to this hypothesis, we age configurations corresponding to state point H in Fig. 2(a) before heating, i.e., at $P=1.38$ GPa and $T=77$ K. The evolution of ρ with time t is shown in Fig. 3. As t goes on, ρ increases approaching the value of ρ corresponding to VHDA at $P=1.38$ GPa. Another support to the hypothesis that VHDA can be interpreted as "relaxed HDA" comes from the study of the effect of the compression T in the LDA$\rightarrow$HDA transformation. If HDA is less stable than VHDA, we should find that (for a given final P after compression of LDA) the larger the compression T, the closer HDA is to the corresponding VHDA. In other words, the higher the compression T of LDA, the more the system can relax to a more stable state. Accordingly, Fig. 2(a) shows that as the compression T is increased, the compression isotherms starting from LDA shift (for a given P) to higher ρ, approaching VHDA.

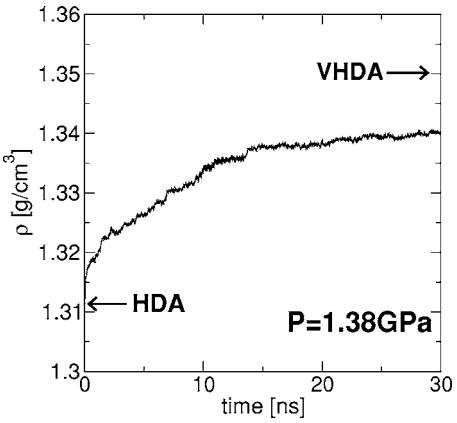

FIG. 3. Effect of aging configurations of HDA corresponding to state point H in Fig. 2(a). With time, the ρ increases approaching the ρ corresponding to VHDA at $P=1.38$ GPa. This finding is consistent with the view of VHDA as the result of relaxation of HDA upon isobaric heating.

B. Heating at intermediate P

We explore now the effect of isobaric heating of the glass at intermediate P, in the LDA-HDA transition region, indicated by state points D, E, F, and G in Fig. 4(a) (see Table I). The lower the P of these HDA forms, the more contaminated they are by LDA. Upon isobaric heating from $T=77$ K up to $T\approx 170$ K, the states indicated by state points D, E, F, and G shift to higher densities as indicated by the arrows in Fig. 4(a). An example of the evolution of ρ upon heating these four glasses is shown in Fig. 4(b). The situation is analogous to the HDA-VHDA transformation discussed above. The increase in T allows these glasses to relax to more stable glass configurations characterized by a higher ρ. The final glasses found after heating at these intermediate P correspond to the "VHDA" obtained at high P's. We note also that at a given intermediate P (e.g., $P=0.8$ GPa), the isotherms obtained in the LDA-HDA transformations shift to higher ρ as the compression T increases. This is because, as discussed in Sec. IV A, the higher the compression T, the more the glass relaxes during compression.

C. Heating at low and negative P

Isobaric heating at P's below the P at which the glass isotherms cross ($P\approx 0.2$ GPa, $\rho\approx 0.98$ g/cm^3) presents

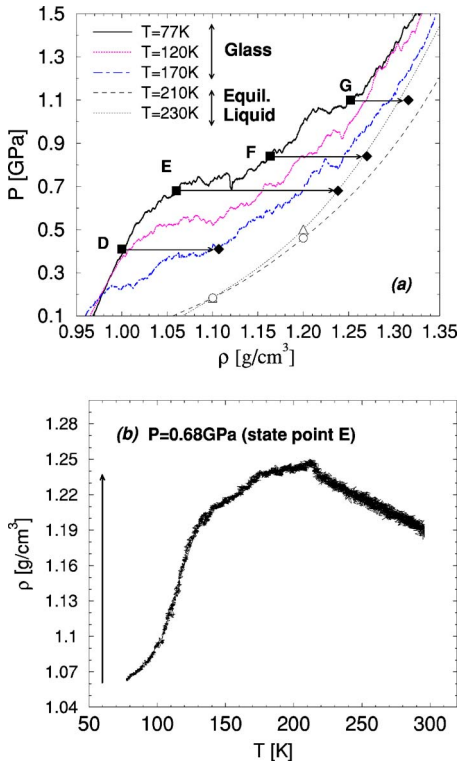

FIG. 4. (Color online) (a) Magnification of Fig. 1 for intermediate densities in the LDA-HDA transition. We heat isobarically glass configurations corresponding to amorphous ices obtained during the transformation of LDA to HDA (state points E, F, G), and one configuration corresponding to LDA (state point D; see also Table I). All state points shift to higher ρ upon heating (see arrows). Squares indicate the ρ of the starting glasses at $T=77$ K while diamonds indicate the final ρ reached at $T\approx 170$ K before the glass transition. We also show the $P-\rho$ values corresponding to two liquid isotherms (from Ref. [18]). (b) Example of the evolution of ρ upon isobaric heating for the four state points D, E, F, and G indicated in Fig. 4(a). The arrow indicates the increase in ρ when heating the glass from $T=77$ K up to $T\approx 170$ K. The smallest increase in ρ occurs for the heating of configurations indicated by state point G and it is larger for heatings at lower P's.

some differences from the cases studied above. We discuss the heating from three LDA configurations indicated by state points A, B, and C in Fig. 5(a) (see Table I). The heating of LDA represented by state point C at $P=0.01$ GPa is shown in Fig. 5(b). We observe a decrease in ρ from 0.96 g/cm^3 at 77 K to $\rho\approx 0.952$ g/cm^3 at $T=150$ K, and then an increase in ρ until $T=230$ K (already in the liquid phase). This behavior of LDA upon heating at $P=0.01$ GPa is consistent with the location of the isotherms in the glassy state. Isotherms in the glassy state shift to lower densities as T increases, suggesting that the more stable glasses at $P=0.01$ GPa are at lower densities. Therefore, the glass represented by state point C moves upon heating first to lower ρ approaching the glass isotherm at $T=170$ K in the glassy state, and then shifts back to higher ρ approaching the $T=230$ K equilibrium liquid isotherm. The relaxed glass obtained before the glass transition is a "very-low density glass" ("VLDA") and is conceptually analogous to the VHDA obtained at high P. A more precise nomenclature for these glasses might be relaxed-LDA (RLDA) and relaxed-HDA (RHDA), respectively (see also [37]).

A situation similar to the one discussed previously for state point C in Fig. 5(a) holds for state point B in Fig. 5(a), i.e., for the isobaric heating at $P=-0.17$ GPa of LDA ($\rho=0.94$ g/cm^3). The ρ upon heating for this case is shown in Fig. 5(c). We observe an initial decrease in ρ down to ≈ 0.93 g/cm^3 at $T\approx 170$ K approaching the value of $\rho\approx 0.92$ g/cm^3 corresponding to the glass isotherm at $T=170$ K. As T increases up to 230 K, a nonmonotonic density dependence arises, probably because the ρ of the equilibrium liquid at $P=-0.17$ GPa and 230 K is also ≈ 0.93 g/cm^3. The final decrease in ρ for higher T is due to the fact that the liquid isotherms at $P=-0.17$ GPa in Fig. 5(a) shift to lower ρ as T increases.

Finally, Fig. 5(d) shows the effect of heating LDA at $P=-0.55$ GPa, indicated by state point A in Fig. 5(a). In this case, ρ decreases abruptly upon heating and LDA transforms into gas (i.e., it "sublimates") because there are no liquid isotherms at this P.

V. RECOVERING OF HDA AND VHDA AT AMBIENT P. A CONTINUUM OF GLASSES

In this section, we investigate the effects of isothermal expansion of HDA and VHDA at low T down to $\rho=0.85$ g/cm^3. The structure of HDA and VHDA has been described at $T=77$ K and $P=0.01$ GPa [27,53]. To compare our results with the experiments, we also recover HDA and VHDA at these conditions. For both HDA and VHDA, the system is decompressed at constant $T=77$ K (in the case of VHDA, we first bring the system back to $T=77$ K by keeping the P constant). We recover the configurations of HDA represented by state points H, I, J, and K in Fig. 2(a), and the corresponding configurations of VHDA.

We first discuss state points H and I, the cases of HDA at $P=1.38$ GPa and $P=1.9$ GPa [see inset of Fig. 6(a)]. State points H′ and I′ are the glasses obtained after heating HDA, i.e., VHDA (≈ 165 K). In agreement with experiments, cooling VHDA back to $T=77$ K increases ρ. The final glasses after cooling, i.e., VHDA (≈ 77 K), are indicated by state points H″ and I″ in the figure. We note that VHDA (≈ 77 K) can be cycled back upon heating to VHDA (≈ 165 K). This is also in agreement with the experimental results [27]. Figure 6(a) shows the evolution of P as a function of ρ during decompression of the system starting at state points H, I (for HDA), H″ and I″ (for VHDA). During decompression, VHDA is denser than the corresponding HDA, and only at $P\approx -0.15$ GPa the densities of the decompressed samples of VHDA are equal.

In experiments, HDA and VHDA recovered at ambient P and $T=77$ K are characterized by only one state with $\rho=1.17$ g/cm^3 and $\rho=1.25$ g/cm^3, respectively. In Figs. 6(b) and 6(c) we show the P during decompression of the four HDA and the four VHDA forms, respectively. The recovered HDA at $P=0$ GPa and $T=77$ K have different densities, and do not collapse to a single state. Also the recovered VHDA forms are characterized by different densities, notwithstand-

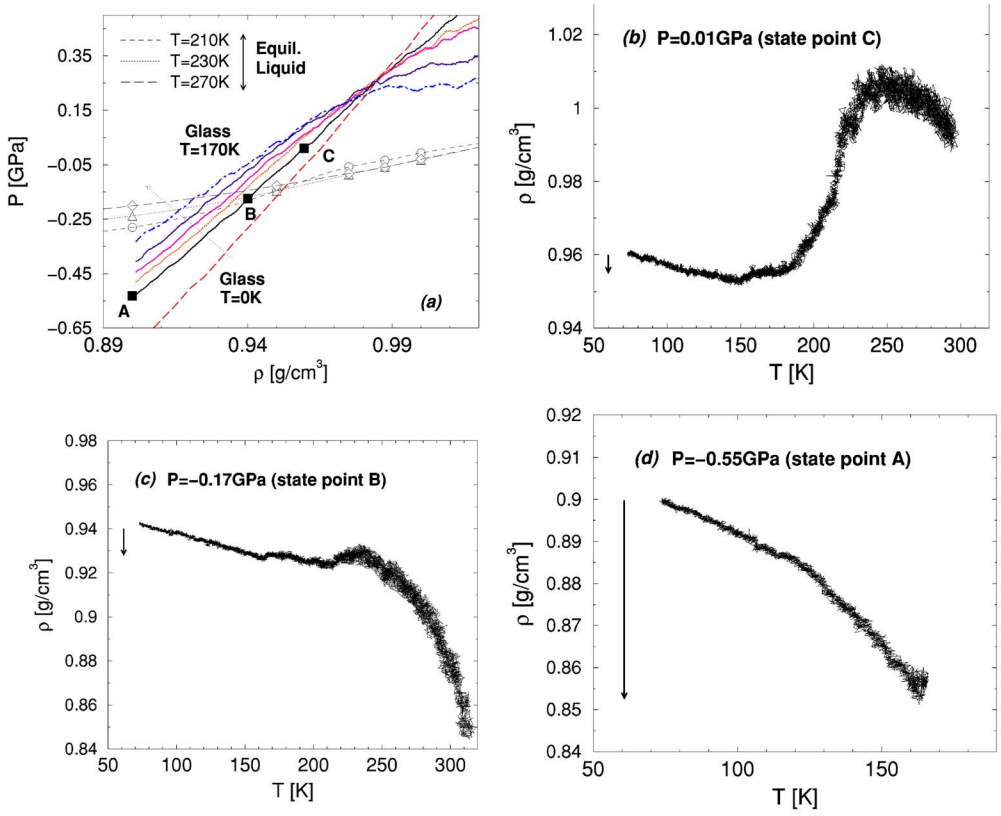

FIG. 5. (Color online) Magnification of Fig. 1 corresponding to densities of LDA. We heat at constant P configurations corresponding to state points A, B, and C in the figure (see also Table I). We show all the glass isotherms simulated corresponding to $T=0$, 77, 100, 120, 140, and 170 K (see dashed arrow), and the liquid isotherms for $T=210$, 230, and 270 K (from Ref. [18]). Note that glass isotherms cross each other at $\rho \approx 0.98$ g/cm^3, $P \approx 0.2$ GPa. After heating and before the liquid phase is reached, state points A, B, and C shift to lower densities. In the three cases, the state points finally approach the liquid isotherm at high T. (b) Evolution of ρ upon isobaric heating at $P=0.01$ GPa [state point C in (a)]. ρ decreases from 0.96 g/cm^3 at 77 K to $\rho \approx 0.952$ g/cm^3 at $T=150$ K (see arrow) and state point C moves through the glass isotherm in (a). Then ρ increases and state point C shifts back to higher densities approaching the $T=230$ K equilibrium liquid isotherm. (c) Evolution of ρ upon isobaric heating the glass up to $T \approx 170$ K at $P=-0.17$ GPa [see point B in (a)], ρ decreases down to ≈ 0.93 g/cm^3 (see arrow). Upon farther heating up to 230 K, ρ does not change much probably because the ρ of the equilibrium liquid at $P=-0.17$ GPa and 230 K is also ≈ 0.93 g/cm^3. (d) Evolution of ρ upon isobaric heating at $P=-0.55$ GPa [see point A in (a)]. ρ decreases monotonically and state point A in (a) shifts to lower densities. The ρ reaches very low values and the glass transforms into gas. Arrow indicates the increase in ρ when heating the glass from $T=77$ K up to $T \approx 160$ K.

ing the same P and T. We observe that at $P \approx 0$ GPa, HDA densities fall in the interval 1.15–1.24 g/cm^3 while VHDA densities fall in the interval 1.22–1.28 g/cm^3. Furthermore, these two ρ intervals overlap, meaning that recovered HDA and VHDA are indistinguishable by their ρ at zero P. It is also clear from our results that there is a continuum of glasses at normal P. A continuum of glasses at normal P has been already suggested by experiments in Refs. [36,37] and obtained in computer simulations using the TIP4P model [31]. Our simulations also show that as P decreases to negative values, all the recovered HDA and VHDA forms collapse to a single state at $\rho=1.05$ g/cm^3 and $P \approx -0.4$ GPa.

VI. RADIAL DISTRIBUTION FUNCTIONS

A. LDA and HDA at normal P

In this section, we study in detail the radial distribution function (RDF) of amorphous ice. We compare the results from simulations and experiments on LDA, HDA, and VHDA. We also investigate how the structure of HDA changes as HDA is transformed to VHDA at high P. The RDFs for glassy water are commonly measured at $T \approx 80$ K and ambient P. In Fig. 7(a) we show the RDF obtained from simulations for LDA ($\rho=0.96$ g/cm^3) and recovered HDA ($\rho=1.2$ g/cm^3) both at $P=0.02 \pm 0.02$ GPa and $T=77$ K. Recovered HDA is obtained by isothermal decompression at $T=77$ K of HDA ($\rho=1.37$ g/cm^3) [state point H in Fig. 6(a)], as discussed in the section above. Figure 7(a) can be compared with Fig. 1 in Ref. [53], which shows the experimental RDF of LDA and recovered HDA at the state point ($P=1$ atm, $T=80$ K). Both figures are very similar. For example, the maxima of $g_{OO}(r)$ for LDA in our simulations are located at 0.27, 0.44, and 0.66 nm, while experimentally [53] they are located at 0.27, 0.45, and 0.68 nm. When going from LDA to HDA by compression, the first peak of $g_{OO}(r)$ increases, the second peak gets wider and smaller, and the third peak shifts to lower values of r. However, for HDA we

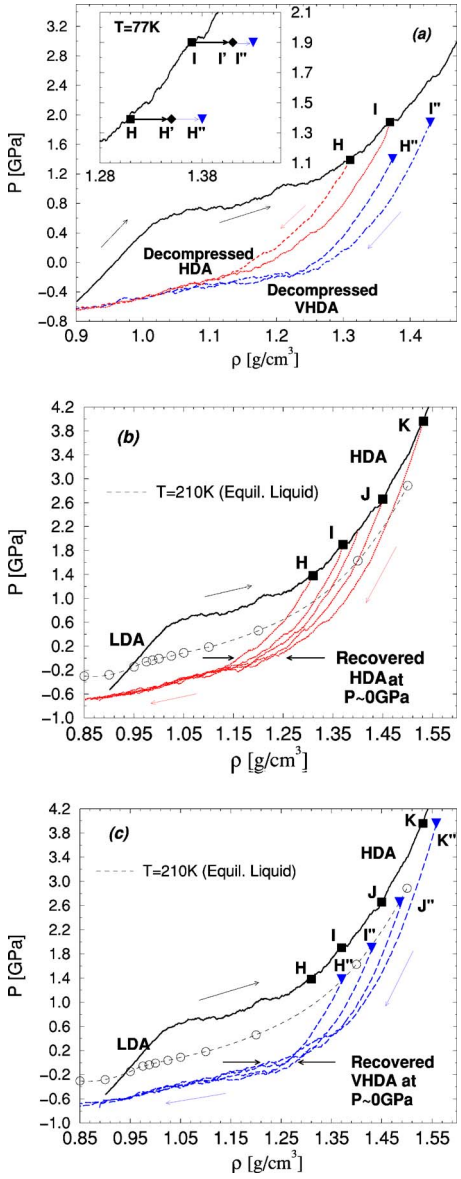

FIG. 6. (Color online) (a) P during decompression of the system starting at state points H, I, H″, and I″. Inset: State points H′ and I′ indicate VHDA configurations at $T \approx 165$ K obtained after heating the HDA configurations represented by state points H and I at $T=77$ K. State points H″ and I″ correspond to the final VHDA states after cooling VHDA back to 77 K. Decompressions at $T=77$ K of (b) the four HDA states indicated by state points (H, I, J, K) and (c) the four VHDA states indicated by H″, I″, J″, K″. At $P \approx 0$ GPa, the recovered configurations of HDA and VHDA do not collapse into two single states but they cover two ranges of densities. HDA densities fall in the interval 1.15–1.24 g/cm^3 while VHDA densities fall in the interval 1.22–1.28 g/cm^3. All recovered HDA and VHDA forms collapse to a single state at $\rho=1.05$ g/cm^3 and $P \approx -0.4$ GPa.

find some differences between experiments and our simulations. The second peak of $g_{OO}(r)$ for our HDA simulations cannot be resolved into two peaks as clearly as in experiments [53], and the first minimum in $g_{OO}(r)$ is located at $r=0.30$ nm instead of at ≈ 0.32 nm. The same observations with respect to the second peak in $g_{OO}(r)$ can be made from

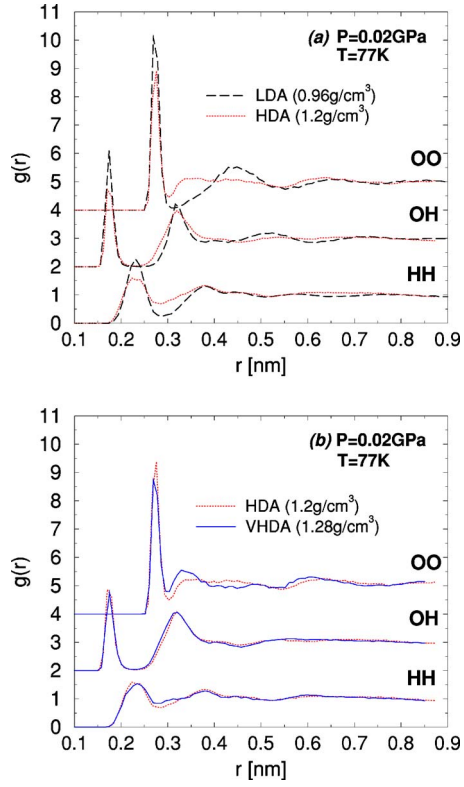

FIG. 7. (Color online) Oxygen-oxygen (OO), oxygen-hydrogen (OH), and hydrogen-hydrogen (HH) radial distribution functions at $T=77$ K and $P=0.02$ GPa for (a) LDA and HDA, and (b) HDA and VHDA. The area under the RDFs indicate that LDA, HDA, and VHDA are characterized by a tetrahedral hydrogen-bonded network and that, in comparison with LDA, HDA has an extra interstitial neighbor between the first and second shell while VHDA has two extra molecules.

MD simulation using the TIP4P model [23,31] and from a reverse Monte Carlo simulation [54]. We note that the second peak of $g_{OO}(r)$ is very sensitive to T; measurements at $P=0$ GPa, $T=100$ K, $\rho=1.16$ g/cm^3 show that the second peak of $g_{OO}(r)$ cannot be resolved into two peaks [55].

The plots for $g_{OH}(r)$ for LDA and HDA in Fig. 7(a) show the same features as those found experimentally in Ref. [53]. When going from LDA to HDA, the first peak of $g_{OH}(r)$ increases, the second peak gets wider, and the third peak practically disappears. However, we note that for both LDA and HDA the relative heights of the first and second peaks of $g_{OH}(r)$ in experiments and simulations are different. Experiments [53] show that both peaks have almost the same amplitude for LDA, while for HDA the *first* peak is smaller than the second one. Instead, SPC/E shows a larger first peak in $g_{OH}(r)$ for both LDA and HDA suggesting that the structure is more tetrahedral than in real water. In accord with experiment [53], for the case of $g_{HH}(r)$ we find an increase of the first peak and decrease of the first minimum of the RDF.

B. HDA and VHDA at ambient *P*

Figure 7(b) shows the RDF of recovered HDA ($\rho \approx 1.37$ g/cm^3) and recovered VHDA ($\rho=1.28$ g/cm^3)

generated as discussed in the previous sections ($P=0.02\pm0.02$, $T=77$ K). VHDA was obtained by isobaric heating of HDA ($\rho\approx1.37$ g/cm^3) up to $T\approx165$ K. Figure 7(b) can be compared with Fig. 1 in Ref. [29], which shows the experimental RDF for recovered HDA and VHDA at ($P=1$ atm, $T=80$ K). In accord with experiments, when going from HDA to VHDA, $g_{OO}(r)$ shows a weak decrease in the first peak and a shift of the third peak to lower values of r. Furthermore, the second wide peak of $g_{OO}(r)$ for HDA practically disappears at $r\approx0.43$ nm. In the experimental $g_{OO}(r)$, the second peak in HDA merges into the first peak, filling the gap at $r=0.33$ nm, the first minimum for HDA. As a consequence, the first peak develops a shoulder with a second maximum at $r=0.35$ nm. In our simulations, this does not occur. Instead, the second maximum is located at $r\approx0.33-0.34$ nm and the first minimum in HDA is not filled, i.e., we still can see a clear minimum in $g_{OO}(r)$ for VHDA. The presence of such a minimum in the $g_{OO}(r)$ for VHDA has been observed also in MD simulations using the TIP4P model [31]. When moving from HDA to VHDA, we find that $g_{OH}(r)$ barely changes. There is a weak shifting of the second peak toward lower values of r as it is found experimentally [29], and the observed decrease of the first peak is barely seen in our simulations. We find that $g_{HH}(r)$ also shows weak changes. As in [29], we find a decrease in the first peak and an increase of the first minimum upon heating.

We expect to find differences in the RDF between experiments and simulations. A comparison of the temperatures of maximum density [42] in SPC/E and in experiments indicates that properties of the SPC/E model at a temperature T correspond to those in experiments at approximately $T'=T+50$ K. Recently, a T shift of -50 K in the T_m of SPC/E has been reported [49]. As we already mentioned, the $g_{OO}(r)$ we find for HDA at $T=77$ K is more similar to that found in experiments at $T=100$ K [55] than the corresponding one at $T=80$ K [53]. Recovering VHDA at higher T will allow neighbor oxygen atoms to come closer, thereby filling the gap at $r\approx0.3$ nm in $g_{OO}(r)$. Therefore, differences between simulations and experiments in the RDF of VHDA are expected to be smaller at higher T.

C. Isobaric heating of HDA to VHDA at high P

In Fig. 8 we show the evolution of the oxygen-oxygen RDF on heating HDA ($\rho=1.37$ g/cm^3) at $P=1.9$ GPa from $T=77$ K up to $T\approx175$ K. Upon heating HDA, the first peak in $g_{OO}(r)$ decreases and molecules move, filling the gap at $r=0.29$ nm. The second peak shifts to lower values of r, merging with the first peak, and the minimum at $r=0.41$ nm decreases. This RDF of VHDA is remarkably similar to the experimental distributions [29] for recovered VHDA at $P=0.02\pm0.02$ and $T=77$ K, suggesting that differences observed in our recovered configurations set up during the decompression process.

D. Coordination number of LDA, HDA, and VHDA

Integration of the experimental $g_{OH}(r)$ at $T=80$ K and normal P for LDA, HDA, and VHDA in the range $0.14\text{ nm}<r<2.5$ nm indicates that each oxygen (O) atom is surrounded by 2 ± 0.1 hydrogen atoms [29,53]. Furthermore, integration of $g_{OO}(r)$ for $r<3.1$ nm [the location of the first minimum in the experimental VHDA $g_{OO}(r)$] indicates that each O has ≈four nearest-neighbor O atoms. Therefore, LDA, HDA, and VHDA are characterized by a tetrahedrally coordinated fully hydrogen bonded network.

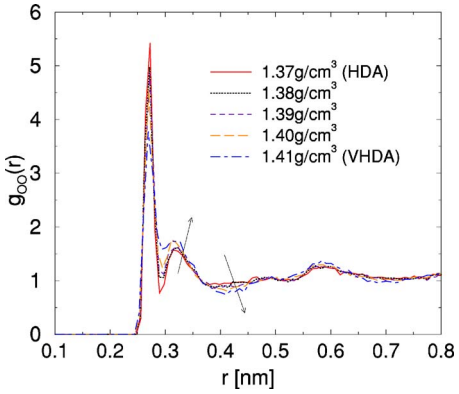

FIG. 8. (Color online) Evolution of the oxygen-oxygen radial distribution functions upon isobaric heating of HDA (1.37 g/cm^3) at $P=1.9$ GPa from $T=77$ K up to $T\approx175$ K.

Our simulations agree with these experimental findings: We find from Fig. 7 that at $P=0.02$ GPa and $T=77$ K in LDA, HDA, and VHDA each oxygen is surrounded by 1.95 ± 0.5 hydrogen atoms (for $r<2.5$ nm) and by 4–4.1 oxygen atoms for $r<0.303$ nm [the first minimum of the simulated $g_{OO}(r)$ for VHDA]. Experiments [29,53] also indicate that differences in structure of HDA and VHDA as compared to LDA basically arise from the presence of extra interstitial neighbors. Integration of the experimental $g_{OO}(r)$ from $r=0.31$ nm [the first minimum of $g_{OO}(r)$ for VHDA] to $r=0.33$ nm [the first minimum of $g_{OO}(r)$ for HDA], indicates that, in this range of distances, an O atom has 0.9 (≈1) oxygen neighbors in HDA and 1.7 (≈2) in VHDA. In simulations, integrating from $r>0.303$ nm [first minimum of $g_{OO}(r)$ for VHDA] up to $r=0.33$ nm, we find that each O atom has 1.1 (≈1) neighbor O in HDA and 1.8 (≈2) in VHDA (in LDA this value is only 0.1). Therefore, simulations are consistent with experiments showing that, in comparison to LDA, there is one extra interstitial molecule in the structure of HDA and approximatively two in the structure of VHDA.

VII. HDA-LDA, VHDA-LDA, AND VHDA-HDA TRANSFORMATIONS

A. HDA-LDA transformation

It was observed by Mishima *et al.* [5] that recovered HDA ($\rho\approx1.17\pm0.02$ g/cm^3) at $T=77$ K and ambient P transforms to LDA ($\rho\approx0.94\pm0.02$ g/cm^3) upon isobaric heating to $T\sim117$ K. In Ref. [23] it is found that simulations at ambient P also show this transition between HDA and LDA. Here we show that our simulations at ambient P show remarkably similar results to those found in [23]. However, we

point out that a direct HDA→LDA transition with the SPC/E model at the present heating rate $q_h=3\times10^{10}$ K/s takes place only at negative P.

Configurations of HDA ($\rho=1.4$ g/cm^3) are obtained by isothermal compression of LDA at 77 K up to $P=2.14$ GPa with a rate of $\partial\rho/\partial t=5\times10^{-5}$ g/cm^3/ps, as explained in Sec. II. HDA is recovered by isothermal decompression at $T=77$ K down to $P\approx-0.7$ GPa with a rate of $\partial\rho/\partial t=-5\times10^{-5}$ g/cm^3/ps [see Fig. 9(a)]. We then heat isobarically recovered HDA ($\rho=1.2$ g/cm^3) at $P=0.01$ GPa. The evolution of the system in the P-ρ plane is indicated by the upper horizontal arrow in Fig. 9(a). $\rho(T)$ upon heating at $P=0.01$ GPa is shown in Fig. 9(b). We observe in Fig. 9(b) that $\rho\approx1.00$ g/cm^3 at $T=220$ K, while the ρ of LDA ($T=77$ K, $P=0.01$ GPa) is ≈0.96 g/cm^3. Therefore, with the present rate $q_h=3\times10^{10}$ K/s, even when the system becomes less dense upon heating, it does not reach the ρ corresponding to LDA at 77 K and 0.01 GPa. A possible explanation of the resistance of HDA to transform into LDA for the SPC/E model at $P=0.01$ GPa (and the facility for which LDA is made at negative pressure) may be the fact that for this model ice I_h is a thermodynamically stable phase only at negative pressures [49]. Simulations using the TIP4P model are similar (Fig. 1 in Ref. [23]). In Ref. [23], the ρ of the system at $T\approx220$ K (during the heating process) is even larger than 1 g/cm^3. The ρ corresponding to LDA in Ref. [23] occurs when $T\gtrsim260$ K and the system is in the liquid phase.

To find the HDA-LDA transition at $P=0.01$ GPa, the system has to "move" in Fig. 9(a) (upper horizontal arrow) from $\rho=1.2$ g/cm^3 to $\rho=0.96$ g/cm^3 crossing liquid isotherms, like the 210 K-liquid isotherm shown in the figure. In the previous paragraph, we show that at the present q_h the system gets trapped at a state with ρ corresponding to the liquid phase at $T=210$ K. It is not clear whether a much slower q_h could allow the system to reach the ρ of LDA. To find a direct HDA→LDA transformation with $q_h=3\times10^{10}$ K/s we heat recovered HDA at negative P's. This is motivated because at $P<0$ the system should cross *first* the glass isotherms *and then* the liquid isotherms to reach the liquid phase. We confirm this view by heating isobarically recovered HDA at $P=-0.3$ GPa [see lower horizontal arrow in Fig. 9(a)]. $\rho(T)$ upon heating is shown in Fig. 9(c) and is consistent with the possibility of a HDA→LDA transformation at $P=-0.3$ GPa, without any liquid intermediate state.

We note that we also repeated the isobaric heating procedure at $P=-0.71$ GPa, where "recovered HDA" (which is already LDA) has a ρ of 0.82 g/cm^3. On isobaric heating ρ decreases abruptly and the glass transforms to gas. In this case, the system on the P-ρ plane moves away from the LDA isotherms and the glass eventually transforms into gas because there are no liquid isotherms at this P.

B. VHDA-LDA transformation

Experiments show that isobaric heating of "recovered VHDA" at $P=0.11$ GPa from $T=77$ K to $T\approx127$ K produces LDA [27]. We test this experimental finding with our simulations by heating configurations of VHDA at

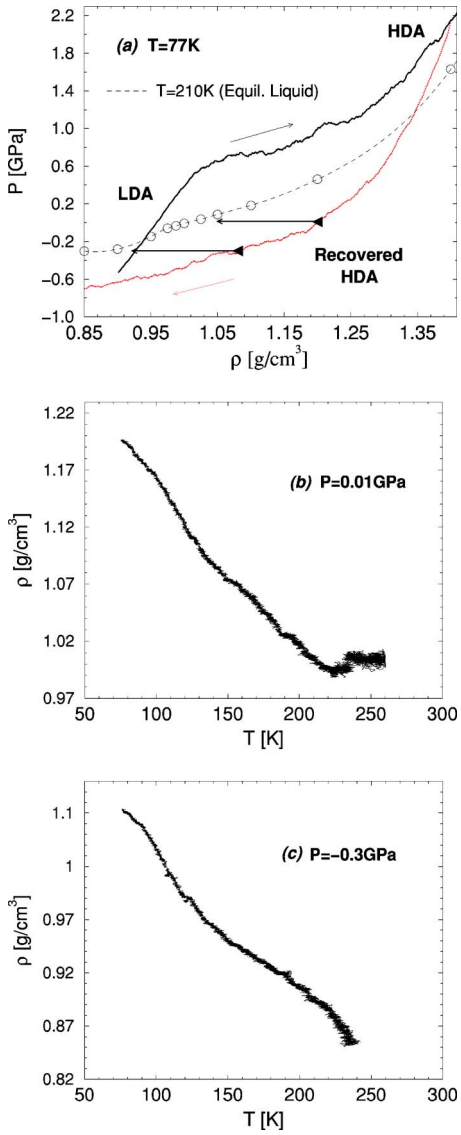

FIG. 9. (Color online) (a) Compression of LDA to obtain HDA, and subsequent decompression of HDA from 1.4 g/cm^3 down to 0.85 g/cm^3. Triangles indicated the starting configurations of recovered HDA at 1.2 g/cm^3, 0.01 GPa and 1.08 g/cm^3, 0.01 GPa that are heated at constant P. The ρ of the system upon heating is shown for (b) $P=0.01$ GPa and (c) $P=-0.3$ GPa. In both cases, the system evolves toward the $T=210$ K liquid isotherm. Arrows in (a) indicate the ρ change upon heating up to $T=170$ K, before the liquid phase is reached. Only the isobaric heating at $P=-0.3$ GPa allows the system to reach the ρ corresponding to LDA (≈0.93 g/cm^3 for this P) supporting the possibility of a HDA→LDA transformation.

$P=0.11$ GPa. We generate VHDA configurations by heating HDA ($\rho=1.31$ g/cm^3, $P=1.38$ GPa) from 77 K to $T\approx160$ K. We then recover VHDA at $T=77$ K, $P=0.11$ GPa, and $\rho=1.27$ g/cm^3.

Upon isobaric heating at $P=0.11$ GPa [see upper horizontal solid arrow in Fig. 10(a)], the system expands as shown in Fig. 10(b). However, the system does not reach the LDA state. For this, the final ρ before the glass transition T should be 0.97 g/cm^3, the ρ of LDA [see Fig. 10(a)]. Instead, Fig.

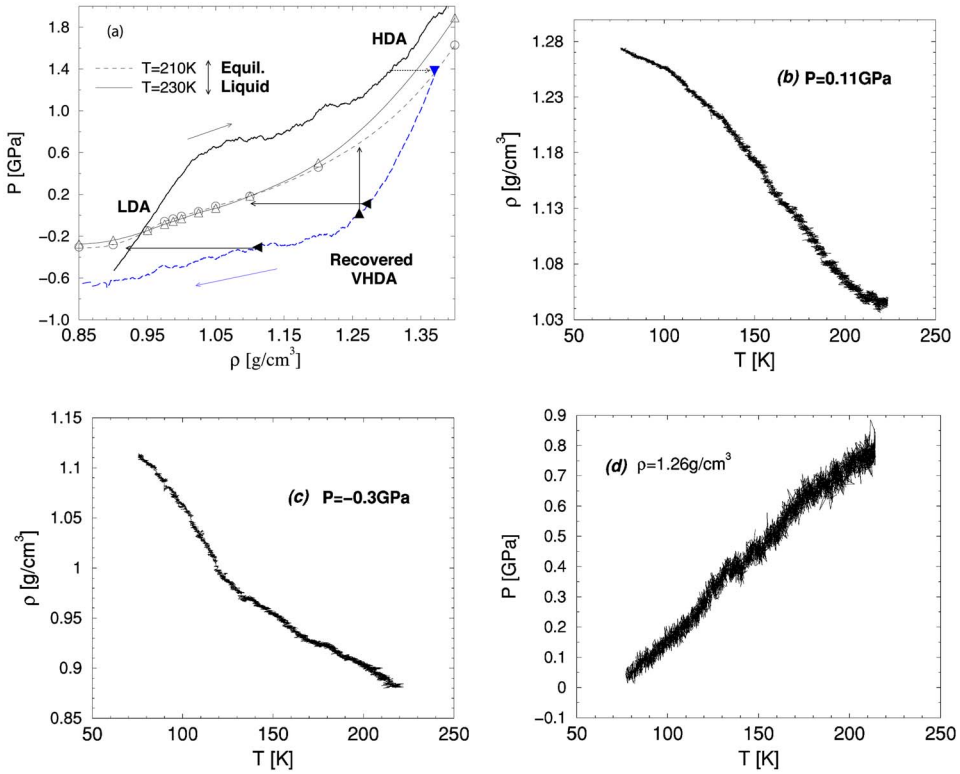

FIG. 10. (Color online) (a) LDA ($\rho=0.9$ g/cm^3) is compressed at $T=77$ K to obtain HDA ($\rho\approx1.31$ g/cm^3). Then, HDA is heated isobarically (horizontal dotted arrow) to obtain VHDA (filled triangle down) and expanded at $T=77$ K (dashed line). VHDA recovered at $\rho=1.27$ g/cm^3 (upper filled triangle left) is heated at constant $P=0.11$ GPa to test whether it produces LDA [see panel (b)]. At this P, the system gets trapped in the liquid phase and no transformation to LDA is observed. VHDA recovered at $\rho=1.11$ g/cm^3 (lower filled triangle left) is heated at constant $P=-0.3$ GPa. The evolution of ρ upon heating [see panel (c)] is consistent with the possibility of a VHDA→LDA transformation. VHDA recovered at $\rho=1.26$ g/cm^3 (filled triangle up) is heated at constant $\rho=1.26$ GPa to test whether it produces HDA [see panel (d)]. The location of the $T=210$ K liquid isotherm avoids a VHDA→HDA transformation (at the present heating rate $q_h=3\times10^{10}$ K/s).

10(b) shows that the ρ at $T\approx170$ K is ≈1.12 g/cm^3, close to the ρ of equilibrium liquid at $T=210$ K and $P=0.11$ GPa—suggesting that the isobaric heating of the recovered VHDA in our simulations brings the system to the liquid state without an intermediate LDA. The situation is similar to the above discussion of the HDA→LDA transformation at $P=0.11$ GPa. The glass upon heating evolves to the liquid phase with no intermediate transformation to LDA. In analogy with the situation of the HDA→LDA transition, a VHDA→LDA transition could be obtained, with the present heating rates, at negative P's, i.e., at P such that the system crosses *first* the glass isotherms *and then* the liquid isotherms. The ρ upon isobaric heating at $P=-0.3$ GPa of recovered VHDA is shown in Fig. 10(c) [see also the lower horizontal arrow in Fig. 10(a)] and it is consistent with the possibility of a VHDA→LDA transformation.

C. VHDA-HDA transformation

Experiments show that isochoric heating of recovered VHDA at $P=0.02$ GPa and $T=77$ K up to $T=140$ K appears to produce HDA [27]. In fact, the x-ray pattern of the final sample has been interpreted as a mixture of VHDA and HDA. We use our simulations to test for the presence of VHDA→HDA transformation by heating configurations of VHDA at constant volume. Configurations of VHDA are obtained by isobaric heating of HDA (77 K, 1.31 g/cm^3) at $P=1.38$ GPa up to $T\approx160$ K. VHDA is then recovered at $P=0.02$ GPa, $T=77$ K, $\rho=1.26$ g/cm^3. The evolution of the system in the $P-\rho$ plane during isochoric heating at $\rho=1.26$ g/cm^3 from $T=77$ K up to $T\sim170$ K is indicated by the vertical arrow in Fig. 10(a). $P(T)$ is shown in Fig. 10(d). P increases monotonically upon heating and approaches the value 0.72 GPa at $T\approx200$ K. At this P and T, the same thermodynamic properties as the equilibrium liquid at $T=210$ K are recovered, as indicated by the liquid isotherm in Fig. 10(a). Therefore, our simulations do not show a VHDA-HDA transformation because the system melts in the liquid phase. The situation is similar to the HDA→LDA transformation at $P=0.01$ GPa discussed above. The P increase during isochoric heating is a consequence of the VHDA→liquid transition.

It is not clear whether a much slower heating rate (nowadays, not accessible in computer simulations [30]) will show a VHDA→HDA transformation or whether such a transformation does not exist. In the short term, experiments may help clarify this issue.

VIII. DISCUSSION

The present study was inspired by several motivations. Among them were (i) the goal of testing how closely simulations based on the SPC/E potential reproduce the experiments, and (ii) the goal of deriving a concise view of the phase diagram of amorphous ice.

We find that even using the simple SPC/E model for water, simulations of isothermal compression of LDA produce another glass, HDA. By repeating the process at different compression T we find that the glass isotherms cross one another in the P-ρ plane. This leads to the different behavior of glassy water at low and high P.

We investigate how under isobaric heating HDA converts into a denser glass VHDA, while under isobaric heating LDA evolves toward a less dense state. The higher the compression T of LDA, the higher the ρ of the final HDA form at a given P, and the closer it is to the corresponding VHDA. This finding is consistent with the view of VHDA as the result of relaxation of HDA upon isobaric heating—i.e., the higher the compression T, the more the glass is able to relax during compression, approaching VHDA. In fact, by aging HDA at high P before heating to obtain VHDA we observe an increase of ρ with time suggesting that VHDA is the result of relaxation of HDA. A similar interpretation of HDA as an unrelaxed glass was proposed by Mishima, when forming HDA by compression of ice I_h at different T [52].

We also investigate the thermal stability of the glasses formed during the compression process of LDA. To do this, we repeat the protocol to transform HDA into VHDA at high P. In other words, we perform isobaric heatings of samples of LDA and samples obtained during the transformation of LDA to HDA. As T increases, irreversible relaxation processes take place generating annealed versions of the starting samples. The resulting annealed glasses (obtained at low and intermediate P) are analogous to the VHDA (obtained at high P).

Densities at different P's and T's for LDA, HDA, and VHDA agree well with experiments. Furthermore, comparison of the structure of these glasses at the level of the radial distribution functions shows differences between the three forms—LDA, HDA, and VHDA—similar to those observed in experiments. In particular, we find that LDA, HDA, and VHDA are characterized by a tetrahedral hydrogen bonded network. As compared to LDA, HDA has an extra interstitial neighbor between the first and second shell while VHDA has two extra molecules.

Stimulated by experimental work, we also simulate the recovering process of different samples of HDA and VHDA at normal P. We find a continuum range of densities for each family of glasses. Furthermore, the ranges of densities of recovered HDA and recovered VHDA overlap at normal P. A continuum of glasses was proposed in Ref. [36] and mentioned as a possibility in Ref. [27].

We discuss the LDA, HDA, and VHDA results with respect to the equation of state of liquid water. The comparison of equilibrium liquid isotherms with those for the glassy state in our simulations allows one to predict the effect of cooling/heating and compression/decompression of amorphous and/or liquid water. For example, one can understand why it is possible to find HDA$\rightarrow$LDA and VHDA$\rightarrow$LDA transformations in SPC/E at $P=-0.3$ GPa and why it is not the case at $P=0.01$ GPa (at least with the present heating rate). We note that experimentally these two transformations to LDA occur at $P\approx 0$ GPa. However, we expect shifts in the values of P, T, and ρ when comparing experiments and simulations. The possible VHDA$\rightarrow$HDA transformation [27] is not observable in simulations with the SPC/E model with the present heating rate.

Some experiments and computer simulations performed in the last few years have challenged the phase diagram proposed in [4,18,19]. Aging effects and the previous history of the glass [especially at $T\lesssim T_g(P)$] make it difficult to characterize the glass state in an unique way. In fact, a glass depends on how it is prepared: Cooling/heating rates, compression/decompression rates, and aging times are variables that have to be included when describing the glass state [48,56]. Therefore, a phase diagram for a metastable system has to be viewed with caution. In the phase diagram proposed in [4,18,19], a first-order transition line separates LDA and HDA at low T, and continues into the liquid phase at high T separating the two liquid phases, LDL and HDL. Furthermore, it has been hypothesized that this first-order transition line ends in a second (metastable) critical point [18,19,21,25,57]. The key points in the phase diagram proposed in [4,18,19] are that LDA is the glass obtained upon cooling of LDL while HDA is the glass obtained upon cooling of HDL. Recent results and simulations call for a refinement of this picture. In [32], we show that VHDA, and not HDA, is the glass obtained upon cooling of HDL. In this modified phase diagram, the first-order transition line between LDL and HDL is continued in the glassy phase separating LDA and VHDA. We note that the properties of the glass obtained upon cooling a liquid can change on the cooling rate [48]. Therefore, VHDA and LDA each represent a family of glasses, all of them obtained upon cooling (with different cooling rates) of HDL and LDL, respectively. Other unrelaxed glasses, e.g., HDA (and probably many other glasses [36] which might depend, for instance, on aging) cannot be shown in a single phase diagram. The phase diagram in [4,18,19] with a *first-order transition line* identifies two distinct liquid phases and the two families of glasses associated to them.

ACKNOWLEDGMENTS

We thank C. A. Angell, A. Geiger, I. Kohl, M. M. Koza, P. H. Poole, A. K. Soper, F. W. Starr, and J. Urquidi for discussions, NSF Grant No. CHE 0096892, and FIRB for support, and the Boston University Computation Center for allocation of CPU time. We also gratefully acknowledge the support of NSF through Collaborative Research in Chemistry Grant No. CHE 0404699.

[1] P. Brüggeller and E. Mayer, Nature (London) **288**, 569 (1980).
[2] P. G. Debenedetti, J. Phys.: Condens. Matter **15**, R1669 (2003).
[3] C. A. Angell, Annu. Rev. Phys. Chem. **55**, 559 (2004).
[4] O. Mishima, L. D. Calvert, and E. Whalley,, Nature (London) **396**, 329 (1998).
[5] O. Mishima, L. D. Calvert, and E. Whalley, Nature (London) **310**, 393 (1984).
[6] M. A. Floriano, J. Chem. Phys. **91**, 7187 (1989).
[7] G. P. Johari, A. Hallbrucker, and E. Mayer, J. Phys. Chem. **94**, 1212 (1990).
[8] O. Mishima, L. D. Calvert, and E. Whalley, Nature (London) **314**, 76 (1985).
[9] O. Mishima, K. Takemura, and K. Aoki, Science **254**, 406 (1991).
[10] M. M. Koza *et al.*, J. Phys.: Condens. Matter **15**, 321 (2003); Phys. Chem. Chem. Phys. **7**, 1423 (2005).
[11] M.-C. Bellissent-Funel, L. Bosio, A. Hallbrucker, E. Mayer, and R. Sridi-Dorbez, J. Chem. Phys. **97**, 1282 (1992).
[12] G. P. Johari, A. Hallbrucker, and E. Mayer, Science **273**, 90 (1996).
[13] D. D. Klug, C. A. Tulk, E. C. Svensson, and C.-K. Loong, Phys. Rev. Lett. **83**, 2584 (1999).
[14] J. S. Tse, D. D. Klug, C. A. Tulk, I. Swainson, E. C. Svensson, C. -K. Loong, V. Shpakov, V. R. Belosludov, R. V. Belosludov, and Y. Kawazoe, Nature (London) **400**, 647 (1999).
[15] P. G. Debenedetti and H. E. Stanley, Phys. Today **56**, 40 (2003).
[16] O. Mishima, J. Chem. Phys. **100**, 5910 (1993).
[17] O. Mishima and H. E. Stanley, Nature (London) **392**, 164 (1998).
[18] P. H. Poole, U. Essmann, F. Sciortino, and H. E. Stanley, Phys. Rev. E **48**, 4605 (1993).
[19] P. H. Poole, F. Sciortino, U. Essmann, and H. E. Stanley, Nature (London) **360**, 324 (1992).
[20] O. Mishima and Y. Suzuki, J. Chem. Phys. **115**, 4199 (2001).
[21] F. Sciortino, E. La Nave, and P. Tartaglia, Phys. Rev. Lett. **91**, 155701 (2003).
[22] S. Engemann, H. Reichert, H. Dosch, J. Bilgram, V. Honkïmaki, and A. Snigirev, Phys. Rev. Lett. **92**, 205701 (2004).
[23] J. S. Tse and M. L. Klein, Phys. Rev. Lett. **58**, 1672 (1987).
[24] S. Harrington, R. Zhang, P. H. Poole, F. Sciortino, and H. E. Stanley, Phys. Rev. Lett. **78**, 2409 (1997).
[25] M. Yamada, S. Mossa, H. E. Stanley, and F. Sciortino, Phys. Rev. Lett. **88**, 195701 (2002).
[26] D. Pascheck, Phys. Rev. Lett. **94**, 217802 (2005).
[27] T. Loerting, C. Salzmann, I. Kohl, E. Mayer, and A. Hallbrucker, Phys. Chem. Chem. Phys. **3**, 5355 (2001).
[28] M. M. Koza, B. Geil, K. Winkel, C. Kohler, F. Czeschka, M. Scheuermann, H. Schober, and T. Hansen, Phys. Rev. Lett. **94**, 125506 (2005).
[29] J. L. Finney, D. T. Bowron, A. K. Soper, T. Loerting, E. Mayer, and A. Hallbrucker, Phys. Rev. Lett. **89**, 205503 (2002).
[30] B. Guillot and Y. Guissani, J. Chem. Phys. **119**, 11740 (2003).
[31] R. Martoňák, D. Donadio, and M. Parrinello, Phys. Rev. Lett. **92**, 225702 (2004); J. Chem. Phys. **122**, 134501 (2005).
[32] N. Giovambattista, H. E. Stanley, and F. Sciortino, Phys. Rev. Lett. **94**, 107803 (2005).
[33] J. Lepault, R. Freeman, and J. Dubochet, J. Microsc. **132**, RP3 (1983).
[34] A. Kouchi and T. Kuroda, Nature (London) **344**, 134 (1990).
[35] G. Strazzulla, G. A. Baratta, G. Leto, and G. Foti, Europhys. Lett. **18**, 517 (1992).
[36] C. A. Tulk, C. J. Benmore, J. Urquidi, D. D. Klug, J. Neuefeind, B. Tomberli, and P. A. Egelstaff, Science **297**, 1320 (2002).
[37] M. Guthrie, J. Urquidi, C. A. Tulk, C. J. Benmore, D. D. Klug, and J. Neuefeind, Phys. Rev. B **68**, 184110 (2003).
[38] O. Mishima and Y. Suzuki, Nature (London) **419**, 599 (2002).
[39] H. J. C. Berendsen, J. R. Grigera, and T. P. Stroatsma, J. Phys. Chem. **91**, 6269 (1987).
[40] F. W. Starr, F. Sciortino, and H. E. Stanley, Phys. Rev. E **60**, 6757 (1999).
[41] S. Harrington, P. H. Poole, F. Sciortino, and H. E. Stanley, J. Chem. Phys. **107**, 7443 (1997).
[42] F. Sciortino, L. Fabbian, S.-H. Chen, and P. Tartaglia, Phys. Rev. E **56**, 5397 (1997).
[43] N. Giovambattista, S. V. Buldyrev, F. W. Starr, and H. E. Stanley, Phys. Rev. Lett. **90**, 085506 (2003).
[44] F. Sciortino, P. Gallo, P. Tartaglia, and S. -H. Chen, Phys. Rev. E **54**, 6331 (1996).
[45] N. Giovambattista, H. E. Stanley, and F. Sciortino, Phys. Rev. Lett. **91**, 115504 (2003).
[46] In much of the previous work on models for water, 216-molecule systems have been employed. Tests with larger systems have confirmed that size effects are numerically irrelevant. In MD simulation studies of glass-glass transition in water, we recall that the LDA-HDA transition has been investigated with a 216-molecule system [19,18,45] and in a 128-molecule system [23], both showing good agreement with experiments. We note that in Ref. [19] it is stated that constant pressure simulations performed with the ST2 potential for water show that the $\rho=0.8$ g/cm^3 isochore obtained for a 1728-molecule system can be reproduced with a 216-molecule system.
[47] N. Giovambattista, C. A. Angell, F. Sciortino, and H. E. Stanley, Phys. Rev. Lett. **93**, 047801 (2004).
[48] N. Giovambattista, H. E. Stanley, and F. Sciortino, Phys. Rev. E **69**, 050201(R) (2004).
[49] T. Bryk and A. D. J. Haymet, J. Chem. Phys. **117**, 10258 (2002); E. Sanz, C. Vega, J. L. F. Abascal, and L. G. MacDowell, Phys. Rev. Lett. **92**, 255701 (2004); C. Vega, E. Sanz, and J. L. F. Abascal, J. Chem. Phys. **122**, 114507 (2005).
[50] E. Whalley, D. D. Klug, and P. Handa, Nature (London) **342**, 782 (1989).
[51] F. W. Starr, S. Harrington, F. Sciortino, and H. E. Stanley, Phys. Rev. Lett. **82**, 3629 (1999).
[52] O. Mishima, Nature (London) **384**, 546 (1996).
[53] J. L. Finney, A. Hallbrucker, I. Kohl, A. K. Soper, and D. T. Bowron, Phys. Rev. Lett. **88**, 225503 (2002).
[54] L. Pusztai, Phys. Rev. B **61**, 28 (2000).
[55] S. Klotz, G. Hamel, J. S. Loveday, R. J. Nelmes, M. Guthrie, and A. K. Soper, Phys. Rev. Lett. **89**, 285502 (2002).
[56] G. P. Johari and O. Andersson, J. Chem. Phys. **120**, 6207 (2004).
[57] A. Scala, F. W. Starr, E. La Nave, H. E. Stanley, and F. Sciortino, Phys. Rev. E **62**, 8016 (2000).